The EMBO Journal (2010) 29, 1055–1068 | © 2010 European Molecular Biology Organization | All Rights Reserved 0261-4189/10
www.embojournal.org

THE EMBO JOURNAL

Force generated by actomyosin contraction builds bridges between adhesive contacts

Olivier M Rossier[1,3], Nils Gauthier[1], Nicolas Biais[1], Wynn Vonnegut[1], Marc-Antoine Fardin[1], Philip Avigan[1], Evan R Heller[1], Anurag Mathur[2], Saba Ghassemi[2], Michael S Koeckert[2], James C Hone[2] and Michael P Sheetz[1,*]

[1]Department of Biological Sciences, Columbia University, New York, NY, USA and [2]Department of Mechanical Engineering, Columbia University, New York, NY, USA

Extracellular matrices *in vivo* are heterogeneous structures containing gaps that cells bridge with an actomyosin network. To understand the basis of bridging, we plated cells on surfaces patterned with fibronectin (FN)-coated stripes separated by non-adhesive regions. Bridges developed large tensions where concave cell edges were anchored to FN by adhesion sites. Actomyosin complexes assembled near those sites (both actin and myosin filaments) and moved towards the centre of the non-adhesive regions in a treadmilling network. Inhibition of myosin-II (MII) or Rho-kinase collapsed bridges, whereas extension continued over adhesive areas. Inhibition of actin polymerization (latrunculin-A, jasplakinolide) also collapsed the actomyosin network. We suggest that MII has distinct functions at different bridge regions: (1) at the concave edges of bridges, MIIA force stimulates actin filament assembly at adhesions and (2) in the body of bridges, myosin cross-links actin filaments and stimulates actomyosin network healing when breaks occur. Both activities ensure turnover of actin networks needed to maintain stable bridges from one adhesive region to another.

The EMBO Journal (2010) **29,** 1055–1068. doi:10.1038/emboj.2010.2; Published online 11 February 2010
Subject Categories: cell & tissue architecture
Keywords: actomyosin dynamics; adhesion; contractile treadmilling; latrunculin; patterned surfaces

Introduction

Distributed throughout the body, connective tissues hold organs in place and are composed of an extensive extracellular fibrous network in which cells are embedded. The extracellular matrix (ECM) is a complex heterogeneous mixture of proteoglycans and protein fibres (collagen, fibronectin (FN) and laminin) that are assembled by cells to structure the tissues. ECM architectures are often discontinuous, comprised of adhesive fibres separated by micron-sized gaps as in the cornea (Nishida *et al*, 1988) or the intestinal mucosa (Toyoda *et al*, 1997). *In vivo*, the ability of cells to sense and respond to the structural heterogeneity of their environment is fundamental for tissue homeostasis. In particular, cell responses to gaps in ECM are of physiological importance during wound closure (Jester *et al*, 1999), but also for regulation of micron-sized fenestra, allowing migration of immune cells through the ECM as in the intestinal mucosa or skin dermis (Desaki and Shimizu, 2000; Stoitzner *et al*, 2002).

In connective tissues, fibroblasts adhere to collagen fibres and develop bridges suspended above the interstices of the fibrous network (Nishida *et al*, 1988; Toyoda *et al*, 1997). Bridging in response to gaps is general as many cell types also exhibit bridges between adhesive fibres in 3D cell-derived or engineered matrices (Rovensky *et al*, 1999; Friedl and Brocker, 2000; Thibault and Buschmann, 2006; Schnell *et al*, 2007; Doyle *et al*, 2009) and above the non-adhesive regions on 2D surfaces (Lehnert *et al*, 2004; Zimerman *et al*, 2004; Thery *et al*, 2006b). Advances in surface patterning (Chen *et al*, 1997) enabled deposition of ECM with a precise geometry on 2D substrates that are ideal for optical microscopy and recapitulate ECM heterogeneity in tissues. Cell spreading on patterned surfaces shows that bridges can form over distances up to 20 μm (Lehnert *et al*, 2004; Zimerman *et al*, 2004). In all situations, bridges are actin-based structures characterized by inwards curved edges (Zand and Albrecht-Buehler, 1989; Jester *et al*, 1994; Thery *et al*, 2006a; Bischofs *et al*, 2008). Bridges are anchored along the edges of the adhesive regions by focal adhesions (FA) (Chen *et al*, 2003; Goffin *et al*, 2006; Thery *et al*, 2006a), which are known to assemble under cytoskeletal tension (Balaban *et al*, 2001; Riveline *et al*, 2001). This suggests that bridges are exerting mechanical tension on their anchoring contacts. However, no direct measurement of forces exerted by bridges has been performed to date.

Traction forces produce cytoskeletal tension and stabilize cell shape. They are powered by non-muscle myosin-II (MII) (Sims *et al*, 1992; Cai *et al*, 2006). Traction forces are stable in time and space despite the rapid dynamics of actin filaments (Galbraith and Sheetz, 1997; Cai *et al*, 2006). Owing to the large distances between adhesions, bridges are structures whose stability could not be explained only by cell-adhesion structures. Bridges contain actomyosin networks that can produce cytoskeletal tension thought to be important for the maintenance of a structured cytoplasm between contacts (Thery *et al*, 2006a).

Contractile filaments that support cytoskeletal tension are remodelled with a rapid turnover (Hotulainen and Lappalainen, 2006). How cells orchestrate turnover with continuous force generation at the molecular level is still unclear? A flowing web of actin and MII could provide cohesion of the cytoplasm as in the cortex of amoeboid cells (Yumura *et al*, 1984). In mammalian fibroblasts,

*Corresponding author. Department of Biological Sciences, Columbia University, Fairchild Center, Room 713, MC 2408, 1212 Amsterdam Avenue, New York, NY 10027, USA. Tel.: +1 212 854 4857; Fax: +1 212 854 6399; E-mail: ms2001@columbia.edu
[3]Present address: CNRS, UMR 5091, Université Bordeaux 2, Bordeaux 33077, France

Received: 8 April 2009; accepted: 5 January 2010; published online: 11 February 2010

however, no similar structure has been reported (Ponti *et al*, 2004; Giannone *et al*, 2007). MII is crucial for actin treadmilling in the lamellipodia in which actin filaments polymerize at the leading edge, flow backwards and depolymerize (Watanabe and Mitchison, 2002; Medeiros *et al*, 2006; Giannone *et al*, 2007). By alignment and organization of actin filaments through contraction, MII is essential for actin dynamics, bundle assembly and the stability of cytoskeletal shape (Sims *et al*, 1992; Wang and Ingber, 1994). However, traction forces are also known to control elongation of FA, which have been shown to be sites of actin polymerization in stress fibres (Hotulainen and Lappalainen, 2006). Such a mode of actin assembly was postulated to depend on MII-based forces, but the level of forces needed was not known (Endlich *et al*, 2007). A corollary of this hypothesis is that MII-generated forces can also regulate either the level or the localization of actin assembly within an existing actin network such as in the bridges?

In mammalian fibroblasts, two isoforms of MII coexist (MIIA and MIIB) and are involved in distinct cellular processes with different localizations (Conti and Adelstein, 2008). For example, MIIA produces the majority of traction forces of mouse embryonic fibroblast (MEF) cells on continuous adhesive substrates (Cai *et al*, 2006) and is responsible for developing a cohesive actomyosin network within the cytoplasm (Cai *et al*, 2010), whereas MIIB is responsible for collagen fibre movement (Meshel *et al*, 2005). In a similar manner, MII isoforms could be used at distinct tasks or in different regions in bridges.

In an effort to unravel the function of contractility in the maintenance of bridges, we used an original force measurement device and found that bridges generated large forces on their anchoring adhesions. When we analysed the dynamics of actomyosin components within bridges on patterned substrates, they showed a treadmilling flow that enabled the replenishment of filaments for continuous force generation. Thus, MII-based contractility was needed for self-sustained cytoskeleton dynamics and maintenance of the cellular bridges, but the two MII isoforms had different functions in the stability of bridges. Bridges were much more dynamic than earlier imagined for a cytoskeleton network of stable filament bundles. Bridges provided a framework to study how cytoskeletal tension, MII contraction, actin polymerization and FA assembly cooperate in an integrated manner to generate a self-sustained stable structure.

Results

Bridges are actin-enriched structures characterized by 'bow-tie'-shaped cytoskeleton with concave edges

To better understand the basis of bridge formation and maintenance, we used patterned substrates with alternating large non-adhesive stripes (polyethylene glycol (PEG) regions of 3.5–20 μm in width) and small adhesive stripes (FN-coated lines of 1.5 to 6 μm in width) (Supplementary data). When MEFs were plated on these surfaces, they spread over adhesive as well as non-adhesive areas (Figure 1A), but extended predominantly along the FN stripes where they developed anchoring FAs (Figure 1B). Cells spanning non-adhesive gaps formed non-adherent bridges that maintained cytoplasmic integrity between adhesions (Figure 1A, box i). Bridges were easily recognized by the concave cell edges over the non-adhesive regions. After 1–2 h of spreading and extension, MEFs reached a fully spread area that was independent of the width of non-adhesive gaps (Supplementary Figure S1) or FN stripes ($A_{TOTAL} = 3219 \pm 98\,\mu m^2$, $n = 193$ for all the patterned substrates tested) with a significant fraction of the cell covering non-adhesive surfaces. We defined a bridging index Br_i as the fraction of total cell area in the bridges: $Br_i = A_{BRIDGE}/A_{TOTAL}$ (e.g. $Br_i = A_{BRIDGE}/A_{TOTAL} = 68.8 \pm 0.8\%$, $n = 14$ for FN line width 4.75 μm, gap 18 μm, with $A_{TOTAL} = 3301 \pm 324\,\mu m^2$). Interestingly, the Br_i of cells on a given pattern was related to the fraction of non-adhesive area on the pattern [f_{NA} = gap width/(gap width + FN stripe width)] and was ranging from 80 to 97% of f_{NA} value.

The actin cytoskeleton was more concentrated in the bridges compared with the adhesive FN stripes (Figure 1A) and assembled into a 'bow-tie' shape in each bridge. The wide parts of the 'bow-tie' were near the concave edges designated type 1 regions where bundles of actin fibres appeared anchored to the edges of FN lines and formed arrowheads. Interestingly, comparing epifluorescence (EPI) and total internal reflection fluorescence (TIRF) microscope images of cytoskeletons in bridges (Figure 1A), we observed that concave edges were significantly above the glass because the actin fibres associated with concave edges appeared only in EPI, but not in TIRF. In the body of bridges defined as type 2 regions, bundles of actin fibres, oriented parallel to the FN stripes, connected the actin arrowheads in type 1 regions on both ends of bridges. The actin meshwork in type 2 regions was more condensed at the centre of the non-adhesive region. There were fewer apparent connections to the FN stripes than in type 1 regions.

FA and strongest traction forces are generated at the sides of concave edges

Organization of FA in cells plated on patterned substrates also confirmed the existence of two types of regions within bridges. FA structures are found only along adhesive stripes (Figure 1B) and are mostly localized at the edges of FN stripes as seen in earlier studies (Chen *et al*, 2003; Thery *et al*, 2006a). Interestingly, the adhesion proteins, paxillin and integrin β3 accumulated with the greatest density along the edges of FN stripes adjacent to concave type 1 regions (Figure 1B). Moreover, FA had different morphologies and orientations in the two regions. In type 1 regions, FA were long and oriented towards the non-adhesive areas, whereas in type 2 regions, FA were dot-like aggregates aligned along the matrix edges, as seen with green fluorescent protein (GFP)-α-actinin (Figure 3A). Type 1 adhesion-rich patches increased in size with the width of the non-adhesive gaps (Supplementary Figure S1). Thus, type 1 regions had the greatest concentration of actin bundles and the largest FA. As FA contacts grow with force (Balaban *et al*, 2001; Riveline *et al*, 2001; Galbraith *et al*, 2002), we postulated that the greatest forces might be concentrated in type 1 regions.

To measure the forces on FA contacts, we fabricated a PDMS pillar device (Tan *et al*, 2003; Cai *et al*, 2006) with rows of force-sensing pillars (2 μm diameter, 5 μm height, spaced by 1 μm with a spring constant: $k = 37.7$ nN/μm) separated with gaps (5–15 μm) similar in size to non-adhesive gaps on patterned substrates (Figure 1C) (Supplementary data). To ensure that cells only adhered to the top of the pillars,

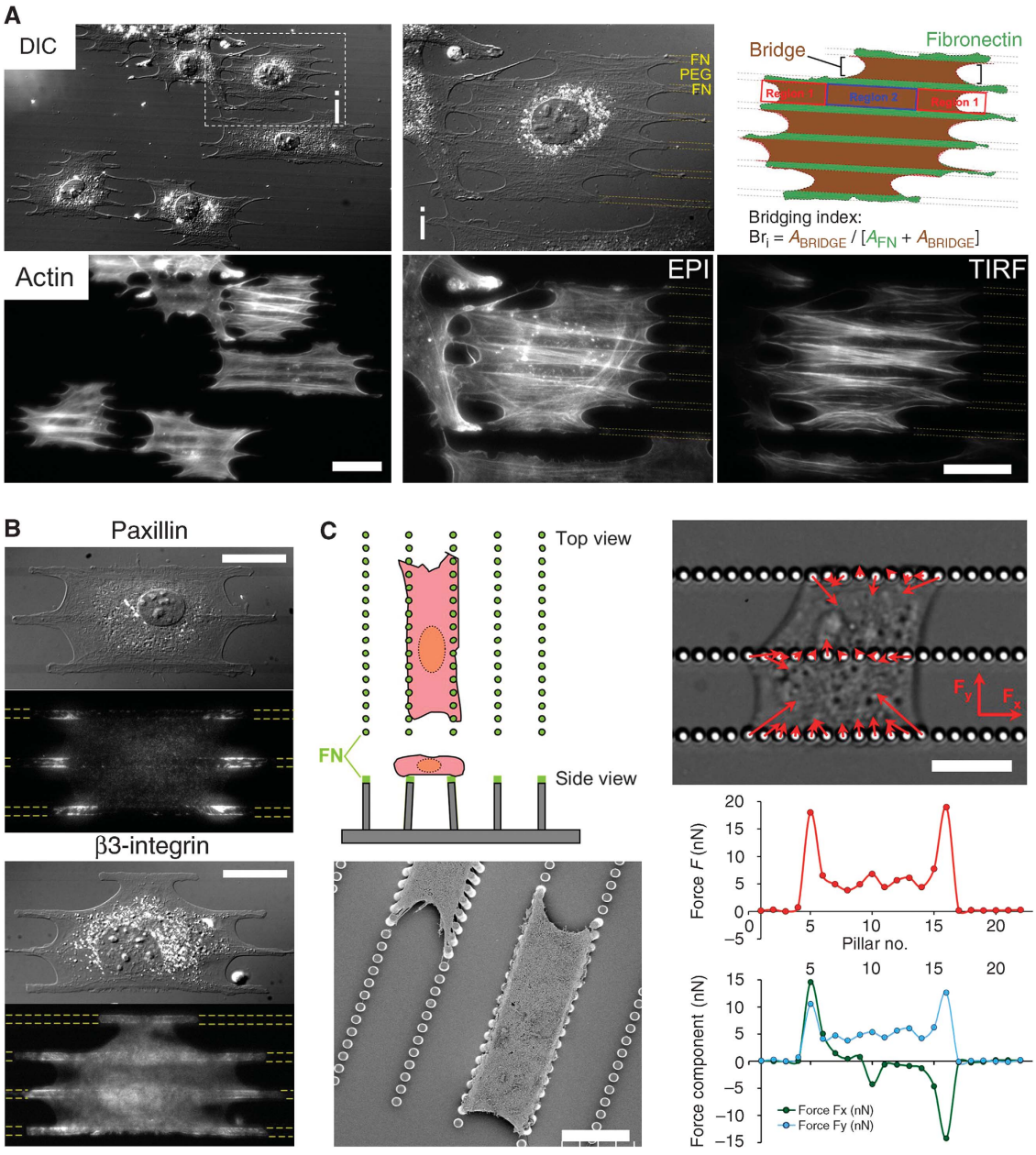

Figure 1 Cellular bridges are actin-rich structures characterized by 'bow-tie'-shaped cytoskeleton and concave edges. FA and strongest traction forces are generated at the sides of concave edges. (**A**) Typical morphology of MEFs spread for 2 h on patterned FN lines. (i) Close-up of cell (i) in the outlined box ($Br_i = 66\%$). Top panel: bridges highlighted in red (A_{BRIDGE}) developed above the non-adhesive regions with arch-shaped ends. The cell regions in contact with FN lines are in green (A_{FN}); bottom panel: actin cytoskeleton in the same cells (EPI and TIRF images). (**B**) Adhesion proteins: paxillin immunostaining by EPI and with GFP-integrin β3 by TIRF. (**C**) Top left: original geometry of PDMS force-sensing pillar device; bottom left: scanning electron micrograph of MEFs onto pillars; top right: differential interference contrast micrograph of MEF exerting onto pillars, traction forces represented with red arrows (force scale bar = 12 nN); bottom right: plot of the amplitude (red circles) of forces exerted on each pillars of the bottom row in the differential interference contrast micrograph, as well as separated force components: Fx along the axis of the rows (green circles) and Fy directed perpendicularly (blue circles). FN lines are outlined with yellow dashed lines. Scale bars: (**A**) 50 μm, **A** (i) 30 μm, (**B**, **C**) 15 μm.

we stamped the tops of the pillars with FN and blocked adhesion to their sides with pluronic F-127 (Supplementary Figure S2). Cellular bridges formed with the same morphology as on the 2D-micropatterned substrates (Figure 1C). We measured the magnitude of the deflection of pillars from their equilibrium position to determine the cell traction forces. The largest traction forces produced by bridges were in the vicinity of the concave edges of bridges (width: 1–4 pillars, i.e. 2–12 μm) with a magnitude of 5–20 nN/pillar (Figure 1C and Supplementary Video 1). Forces were directed parallel to the concave edges along the anchored actin bundles in region 1. In type 2 regions, forces were oriented perpendicular to the rows of pillars and were smaller. When pillars were pulled by two adjacent bridges, they often had no deflection or a deflection parallel to the rows of pillars, resulting from the sum of the forces from both bridges. We conclude that FA size and orientation correlated with the traction forces and further established the differences between regions 1 and 2.

In particular, the concave region 1 had the highest forces and seemed to contribute to bridge development.

Formation of bridges correlates with actomyosin assembly and contractions

To understand the steps that led to extension of bridges, adhesion localization and force generation in bridges, we studied how cells spread and expand their area on patterned substrates. At early stages, MEFs rapidly spread regardless of the substrate coating and then abruptly started MII-dependent contractions as described earlier on continuous adhesive substrates (Giannone *et al*, 2004). Contractions caused inwards bowing of cell edges over the non-adhesive regions, while outwards extension continued over the adhesive regions (Figure 2A and Supplementary Video 2). Live-cell imaging of β-actin (GFP-β-actin) and MII regulatory light chain (GFP-MRLC that binds to all the isoforms of the MII heavy chain) revealed that actin and MII were preferentially recruited above non-adhesive areas as contraction started (Figure 2A and Supplementary Videos 3 and 4). As a consequence, there were stronger forces in between FN stripes than along them. After MII recruitment, actin filaments bent inwards, while staying anchored at their ends to the sides of concave edges (Figure 2A, box ii), and over time, MII fibres contracted to the middle of the non-adhesive regions (Figure 2A, box iii). Thus, the 'bow-tie' shape of bridges over non-adhesive regions appeared to be caused by actomyosin contraction.

After the initial spreading, cells expanded their projected area through extension of existing bridges. They extended through cycles of protrusions and contractions along the FN lines (Figure 2B and Supplementary Video 5) (Giannone *et al*, 2004). Contractions formed adhesions at sites further along the FN stripe that grew as the concave edge extended. Originating from FN stripes, protrusions above non-adhesive areas were rich in actin, but contained very diffuse MII (Figure 2B, arrow). They ruffled back along the curved edge of the bridge except near new FA sites where they

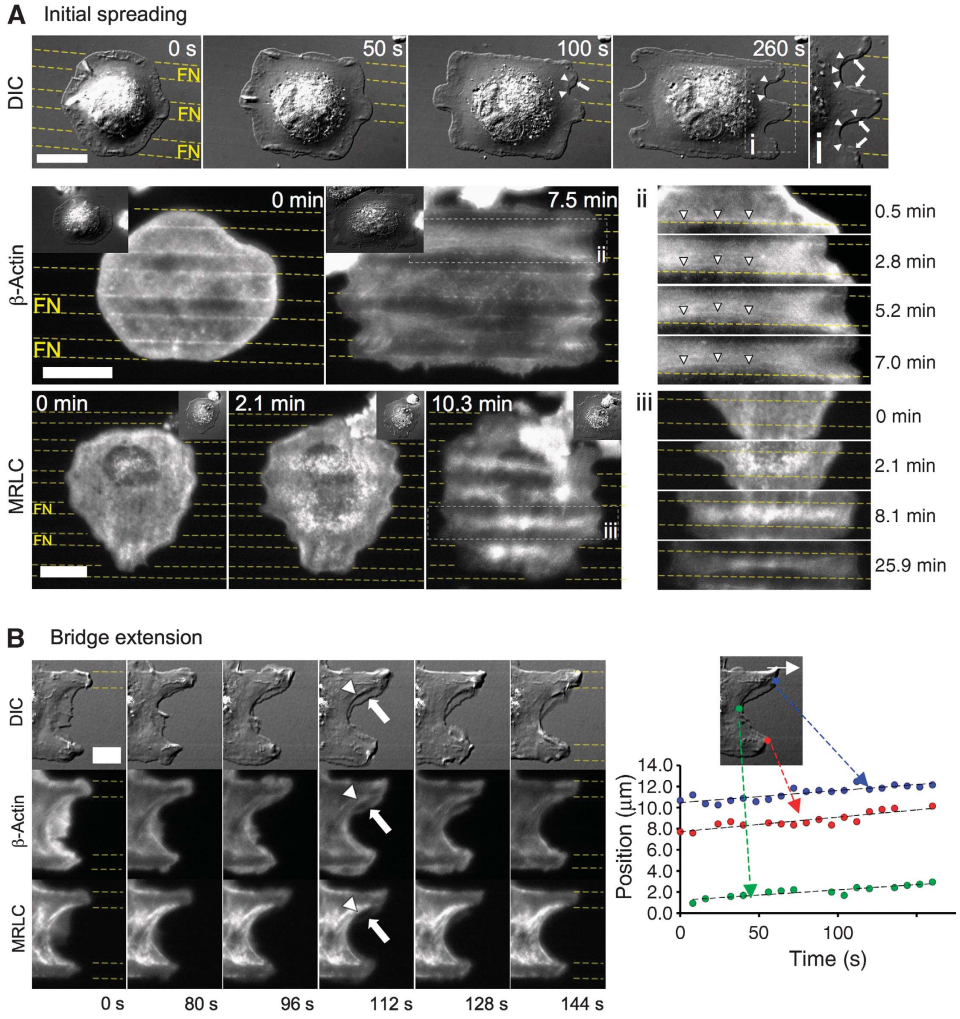

Figure 2 Formation and extension of bridges correlate with actomyosin assembly and contractions. (**A**) Differential interference contrast: formation of arch-shaped edges (arrowheads) during late spreading on a patterned substrate. Arrows indicate coexisting transient protrusions. GFP-β-actin (TIRF): when bridges formed (2.8 min), actin cables bent towards the middle (box ii, arrowheads, 7.0 min). GFP-MRLC (TIRF): when bridges formed, MRLC is enriched above non-adhesive regions and condensed into bow-tie-shaped fibres at longer times. (**B**) Bridge extension during a cycle of extension of actin-rich protrusions (arrow) followed by contraction into MII bundles (arrowhead). Plot of positions of FN-attached regions (blue and red dots) and bridge edge (green dot) versus time during one cycle. Scale bars: (**A**) 15 μm (except for differential interference contrast panel: 18 μm) and (**B**) 13 μm.

provided links to the actomyosin network in the concave region. Actin filaments then condensed into thick cables that colocalized with GFP-MRLC in the concave edges (Figure 2B, arrowheads). Such thickening of actin filaments correlated with an enhanced concentration of MII (Supplementary Video 5). Bridge extension relied on extension of FN-attached regions and followed them with the same velocity (Figure 2B).

After 1–2 h of spreading and extension, MEFs reached a fully spread area. Interestingly, during the whole process of cell spreading and extension to the final spread area, the bridging index Br_i stayed constant ±7% (Figure 4C).

Actomyosin dynamics within bridges exhibit two distinct patterns: (1) 'contractile' treadmilling at the concave edges and (2) 'cross-linking' in the body of bridges

To study actomyosin dynamics in bridges, we followed α-actinin, an actin binding protein and MRLC. Actomyosin dynamics in bridges showed two different behaviours in the two distinct regions of the 'bow-tie'-shaped cytoskeleton. Both proteins were found to label intensely the 'bow-tie' cytoskeleton (Figure 3A and B and Supplementary Videos 6 and 7). Speckles of GFP-α-actinin were tracked as fiduciary markers and analysed by particle image velocimetry to obtain the velocity fields (Figure 3A). In the vicinity of the concave edges (width 5–30 μm), GFP-α-actinin speckles originated from the adhesion-rich patches located at the FN borders and flowed with velocities between 4 and 10 nm/s towards the middle of the non-adhesive region, indicating treadmilling of actin from the edges of FN stripes to the centre of the non-adhesive region. GFP-MRLC speckles also formed at the border of FN stripes by FA sites and flowed with similar velocities as GFP-α-actinin speckles to the centre of non-adhesive regions, indicating that concave regions 1 were continuously contracting (Figures 3B, box i and 7A, box ii and Supplementary Videos 7 and 14). We suggest that this dynamic pattern common to both GFP-α-actinin and MRLC speckles is indicative of actomyosin 'contractile' treadmilling.

In the middle section of bridges (region 2), within the actin bundles, GFP-α-actinin and GFP-MRLC speckles oscillated in synchrony without net movement (α-actinin: Figures 3A and 5B and Supplementary Videos 6 and 9; MRLC: Figure 3B, box ii and Supplementary Video 7). Owing to their function in maintaining connections across the cell, actomyosin bundles in region 2 appear to be supporting high tensions and oscillations in the contractions gave rise to the fluctuations in position as in a tug of war. Occasionally, fibres appeared to rupture causing the aggregates near the 'break' to separate as previously seen for surgically broken stress fibres anchored to mature FA (Rajfur *et al*, 2002; Kumar *et al*, 2006) (Figure 7A and Supplementary Video 14). However, contrary to the latter case, there was rapid healing of the ruptures. After an initial rapid separation, movement of GFP-MRLC aggregates slowed and new aggregates formed in the gap that restored normal density (Figure 7A, red arrowheads, box i). Oscillation of the new aggregates around their initial positions indicated that mechanical continuity of the network was restored (Supplementary Video 14).

In newly formed bridges, actin dynamics presented only 'contractile' treadmilling flow patterns as found in region 1 (Figure 3A, bottom bridge and Supplementary Video 6). This indicated that the actin dynamics in region 2 only appeared when the concave edges moved sufficiently far from each other.

Contraction and force generation by MII is essential for the formation and maintenance of bridges

Actomyosin dynamics could have been governed by two major factors: contraction mediated by MII and/or actin polymerization. To test whether MII contractility was involved in maintenance of bridges, we added blebbistatin (BBI), an inhibitor of MII ATPase activity (Straight *et al*, 2003), to spread cells with established bridges. After 2 min

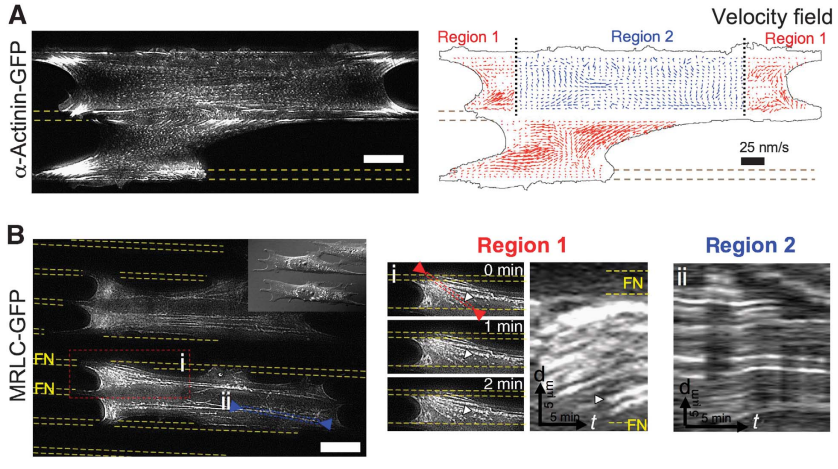

Figure 3 Actomyosin dynamics within bridges exhibit two distinct patterns, (1) 'contractile' treadmilling at the concave edges of bridges and (2) 'cross-linking' in the body of bridges. (**A**) GFP-α-actinin (TIRF): speckles decorated the 'bow-tie'-shaped actin cytoskeleton as well as FAs; velocity field: particle image velocimetry analysis of speckles' dynamics permitted to define a 'contractile' treadmilling pattern (region 1-red arrows) at concave edges of mature bridges and in newly formed bridges, and a 'cross-linking' pattern (region 2-blue arrows) in the body of bridges. Velocity scale bar = 25 nm/s. (**B**) GFP-MRLC (TIRF): similar dynamical patterns were observed with MII ongoing (i) 'contractile' treadmilling in region 1 as seen with MRLC speckles in snapshot (arrowhead) and in kymograph taken along the red line (arrowhead: corresponding speckle trajectory) and (ii) 'cross-linking' dynamics in region 2 as seen in kymograph of MRLC speckles along actin fibre (blue line ii). Images were filtered with the ImageJ plugin SpotTracker. Scale bars: (**A**, **B**) 15 μm.

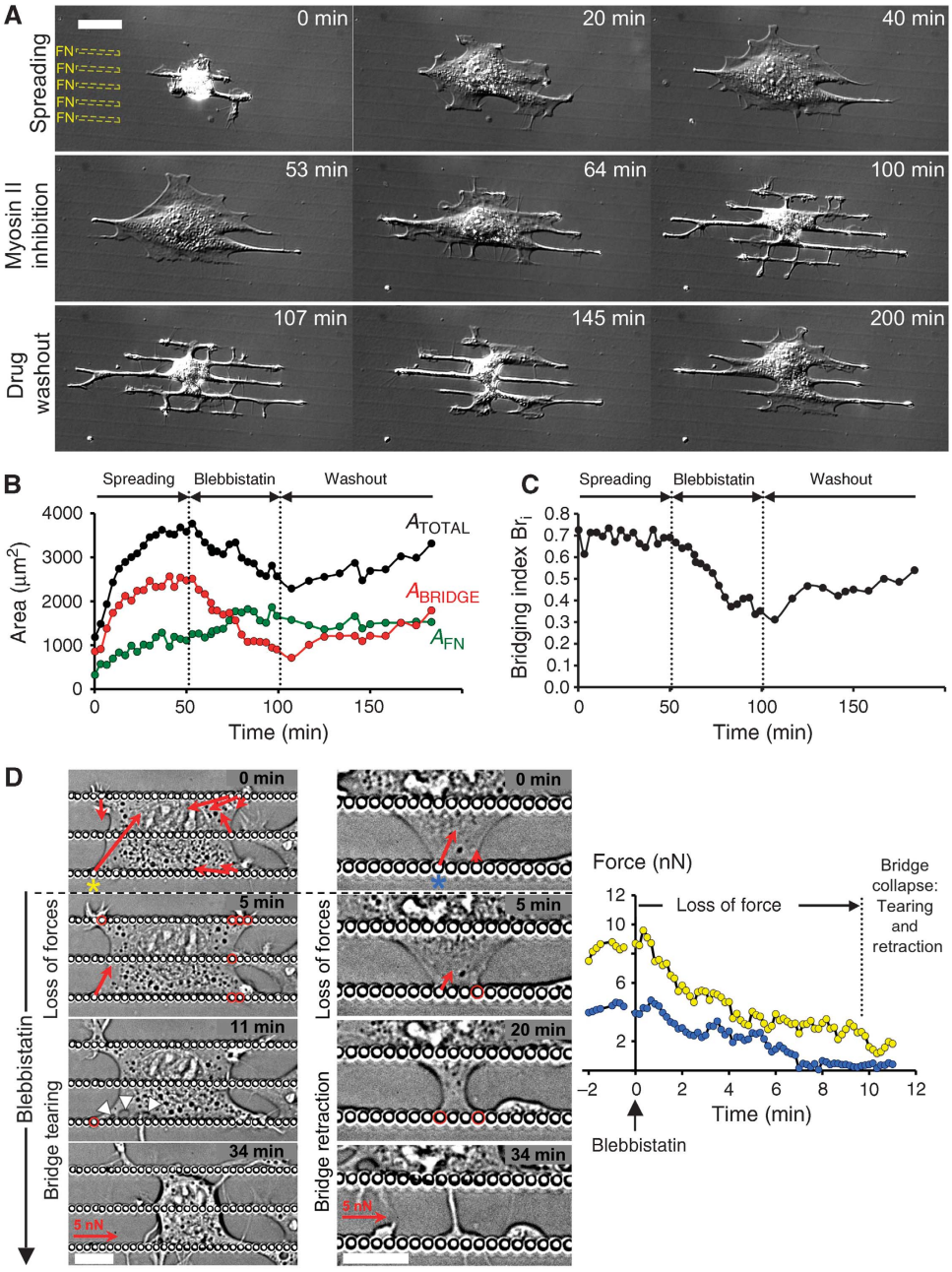

Figure 4 Generation of forces induced by MII activity is essential for the formation and maintenance of bridges. (**A**) Reversible collapse of bridges induced by MII inhibition with MEF initial spreading ($t = 0$ to 40 min), perfusion of BBI ($t = 50$ to 100 min), and drug washout ($t = 100$ min). (**B**) Plot of the variation versus time of the total projected area, A_{TOTAL} (black circles), the bridge area, A_{BRIDGE} (red circles) and the cell area above the adhesive region, A_{FN} (green circles), for the cell depicted in (**A**). (**C**) Plot of the variation versus time of the bridging index, Br_i (black circles), for the cell depicted in (**A**). Br_i was constant during cell spreading and decreased from 69 to 32% during BBI perfusion. (**D**) During BBI treatment, force generation by bridges represented with red arrows (force scale bar = 5 nN) stopped after 5–10 min (red circles indicated pillars where force generation was stopped); then bridge tearing (left panel: arrowheads) and/or bridge retraction (middle panel) led to bridges' collapse. Plot of the variation during BBI perfusion versus time of the traction force exerted on pillars adjacent to the concave edges (marked by asterisks: yellow for pillar in left panel and blue in middle panel). Scale bars: (**A**) 30 μm and (**D**) 15 μm.

of BBI application, bridges started to collapse into thin tubular processes that were complete in <30 min (Figure 4A and B and Supplementary Video 8). No retraction fibres (Mitchison, 1992) were left, reinforcing the suggestion that there were no adhesions in non-adhesive areas. In addition, the perinuclear region rounded as the cytoplasm retracted. However, the frequency and duration of extensions from or along the FN stripes seemed unchanged. Further, cellular extension along FN stripes increased (Figure 4B). In addition, in separate experiments, MII inhibition did not block initial spreading along the FN stripes or across non-adhesive areas. However, after initial spreading, bridges did not form even though processes extended along the adhesive stripes and across non-adhesive regions (data not shown). Seven to ten minutes after BBI was removed, the bridges started to reform slowly as evidenced by a Br_i

increase (Figure 4C), and perinuclear cytoplasm extension with nuclear flattening. Inhibition of the Rho-associated kinase (ROCK), an upstream activator of MII, with the drug Y-27632 caused similar disruption of bridges.

To determine the relationship between MII and force generation by bridges, we measured forces generated by cells on pillars during MII inhibition with BBI. MII inhibition caused gradual loss of force over 5–10 min after the drug application, similar to the time course of the initial loss of bridges (Figure 4D). The collapse of the bridges occurred as on patterned substrates (Supplementary Video 8) either by tearing the structures from the adhesive pillars in the contractile regions 1 or gradual retraction of the concave edges (Figure 4D). Thus, generation of contractile force by MII was critical for the formation and maintenance of bridges and seemed to be the upstream signal in bridge maintenance.

To quantify the function of MII in the formation of bridges, we measured the bridging index after 90 min of MII inhibition (Supplementary Figure S3). After BBI or ROCK inhibitor treatment, Br_i dropped dramatically (control: $68.8 \pm 0.8\%$, $n = 14$; BBI: $36.2 \pm 3.6\%$, $n = 10$—P value $= 6 \times 10^{-6}$ and Y-27632: $49.6 \pm 2.7\%$, $n = 12$ cells—P value $= 2 \times 10^{-5}$; P values are calculated versus control), whereas myosin light chain kinase (MLCK) inhibition with the drug ML-7 had little effect (ML-7: $63.7 \pm 2.0\%$, $n = 12$ cells—P values $= 4 \times 10^{-2}$ versus control). Thus, we suggest that the MII activity involved in forming and stabilizing bridges is mediated by a ROCK-dependent pathway.

MII activity increased actin filament assembly at the adhesion sites and cross-linking of actomyosin filaments in the body of bridges

To understand how the cytoskeletal structures were regulated by MII activity, we followed actomyosin dynamics through actin, α-actinin and MRLC dynamics in bridges after MII was inhibited by BBI. During the collapse of bridges, actin cables spanning above non-adhesive areas were not simply detached from FN stripes and dragged by the retracting concave edges, but actually disassembled (Figure 5A). This observation led us to ask how is MII contraction related to actin dynamics, potentially through assembly and turnover? And more specifically, how did the 'cross-linking' and 'contractile' actomyosin treadmilling get disrupted?

In the middle part of bridges (region 2), standard oscillations of GFP-α-actinin and MRLC speckles stopped within 10 min after BBI perfusion (Figures 5B and 7A). Fibrous arrays dissociated into groups of aggregates that moved away from each other. Interestingly, GFP-α-actinin speckles appeared initially to be sliding apart along the actin bundles indicating tearing of cytoskeleton and relaxation of an elastic

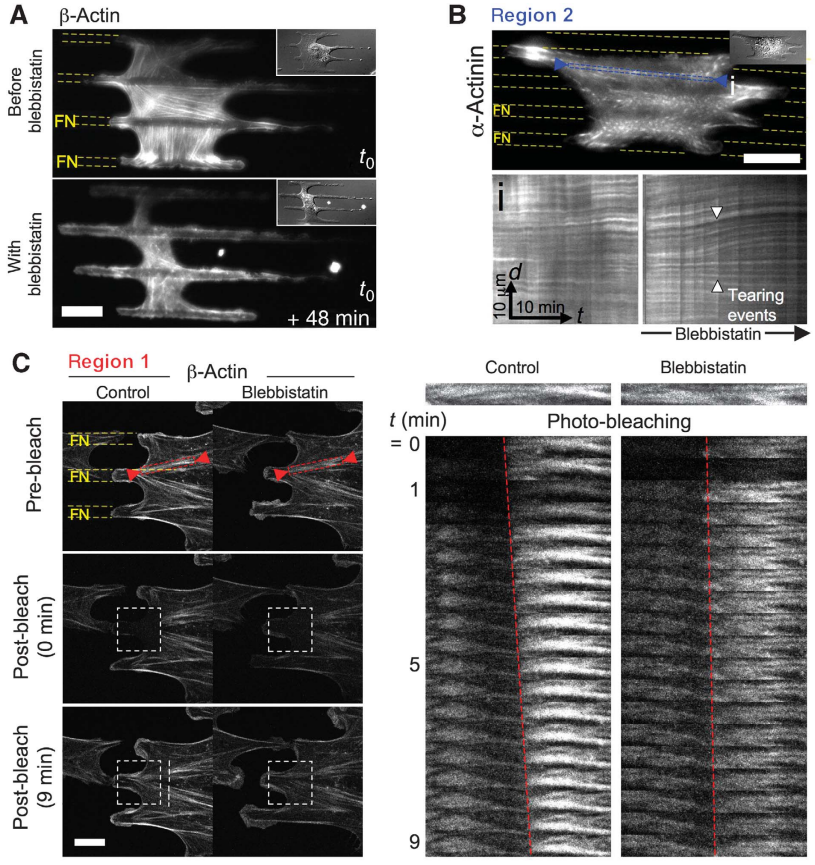

Figure 5 MII activity increased actin filament assembly at the adhesion sites and cross-linking of actomyosin filaments in the body of bridges. (**A**) GFP-β-actin (TIRF): under BBI treatment, actin cables within the bridge vanished concomitantly with the decrease of A_{BRIDGE} and with further expansion on FN stripes. (**B**) GFP-α-actinin (TIRF) speckles dynamics in the actomyosin bundles in region 2 during BBI treatment as seen in kymograph (box i) taken along actomyosin fibres (blue line i). (**C**) FRAP experiment with GFP-β-actin. Left: GFP-β-actin in region 1 was photo-bleached in a square of 12 μm side (white square with dashed lines) in the same cell for two different conditions: left panel represents the control case; right panel shows the case of the same cell treated with BBI. Dashed white segments outlined in the control case the new position of the photo-bleached actin bundles that moved away from their anchoring point. Right: montage of the actin bundles inside the red rectangles (15.2×1.8 μm) for the two conditions. Scale bars: (**A**) 18 μm, (**B**) 15 μm and (**C**) 8.5 μm.

component (Supplementary Video 9). Furthermore, healing processes ceased when MII was inhibited (Figure 7A, box i and Supplementary Video 14). Simultaneously with breakage of bundles, actomyosin movements in bundles decreased to a level in which components appeared frozen. Those observations indicated that actomyosin cables in the body of bridges required MII tension to maintain actin filament linkages within bundles.

To follow the disruption of 'contractile' actomyosin treadmilling within the bundles in the concave regions 1, we used FRAP of GFP-β-actin in cells spread on FN stripes to analyse the actin dynamics before and after BBI addition (Supplementary data and Figure S4). When we performed FRAP on a concave region near the curved cell edge and FN adhesions (Figure 5C and Supplementary Video 10), the photo-bleached boundary of the actin bundles moved away from the anchoring point on the FN stripe into the non-adhesive area with a velocity of 0.26 ± 0.07 μm/min ($n = 8$) (Figure 5C). Fluorescence recovered by localized growth from FA sites with similar rates (0.21 μm/min) superimposed on a simultaneous general recovery of fluorescence within the photo-bleached area (the result of actin turnover within the bundles). This confirmed the existence of actin treadmilling, as similar observations were made initially with GFP-α-actinin.

After adding BBI, fluorescence recovery within bundles in region 1 was strikingly altered. Treadmilling flow of the actin bundles was reduced dramatically (velocity = 0.08 μm/min) (Figure 5C). In addition, inwards movement of MRLC aggregates from the FN edges to the middle of the non-adhesive area slowed dramatically from 0.54–0.6 to 0.06–0.12 μm/min (Figure 7A, box ii). Loss of the 'contractile' actomyosin treadmilling pattern after BBI addition paralleled the loss of force before the bridges collapsed (Figure 4D). Interestingly, the fluorescence recovery within actin bundles was not stopped, but occurred homogeneously without directed elongation from the adhesive area or translocation of the bleached area. This indicated that the MII-mediated contractile forces induced the treadmilling movement of the actin and associated MII components through increased actin assembly at the adhesion-rich sites. Actin turnover within bundles of actomyosin filaments appeared to be preferentially localized to specific sites (FA sites) by a force-dependent mechanism that is superimposed on a force-independent filament exchange that remained during BBI treatment.

Latrunculin-A treatment revealed two different actomyosin meshworks in bridges

Further support for the hypothesis that force generation was involved in regulating the localization of polymerization came with pharmacological inhibition of actin polymerization. Addition of latrunculin-A (LA) to decrease monomeric g-actin without affecting MII contractility had an effect on cell bridges very similar to BBI (Figure 6A, Br_i dropped from 69 to

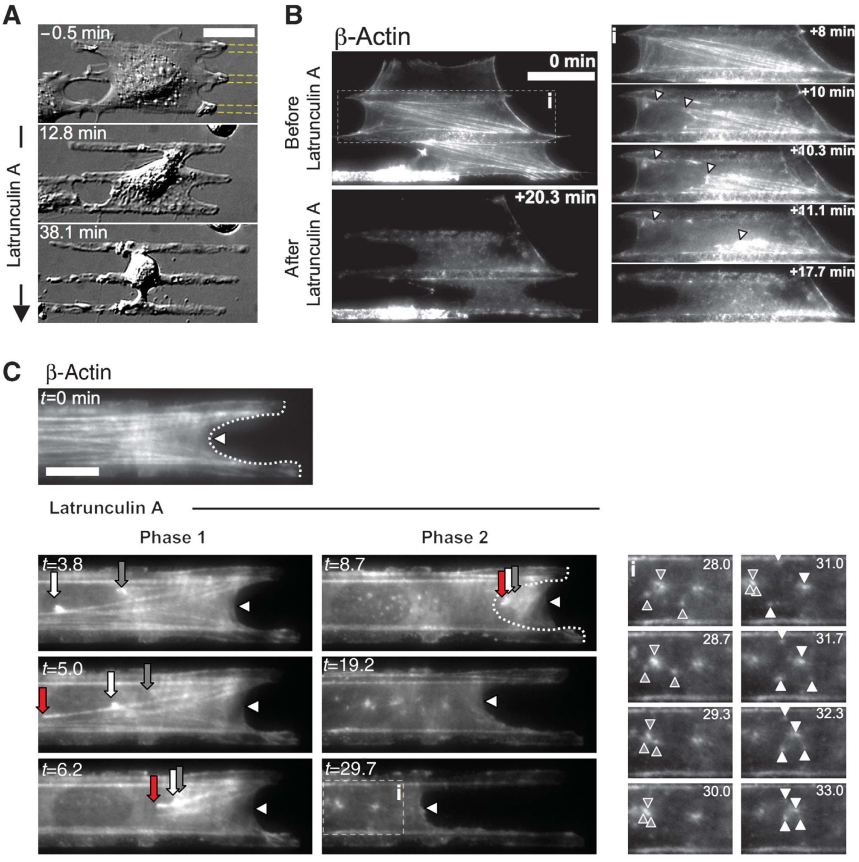

Figure 6 LA treatment disrupts in a two-step process the two actin networks in bridges. (**A**, **B**) LA treatment (applied at $t = 0$ min) disrupts bridges by detachment of the bow-tie actin network from the borders of the FN stripes (white arrowheads). (**C**) LA treatment (applied at $t = 0$) showed two distinct steps: phase 1-actin network detachment from the FN stripes with rapid actin fibres condensation (red, grey and white arrows) followed by phase 2-slow bridge retraction (arrowhead) during which the remaining diffuse actin meshwork contracts and displays actin asters formation and interaction (box i). Scale bars: (**A**, **B**) 30 μm and (**C**) 15 μm.

20% and Supplementary Video 11). After LA was added, bridge collapse started early on and proceeded more quickly than during BBI treatment. The sequence of events during LA-induced collapse of bridges further supported a mechanism of force-dependent growth at FA sites, as the first event visible by both differential interference contrast and live imaging of β-actin-GFP was detachment of the actin network from the borders of FN stripes in region 1 (Figure 6 and Supplementary Videos 11, 12 and 13). This supported the hypothesis that those sites were primary sites of force-dependent actin filament assembly. This detachment was accompanied by a rapid condensation of the bow-tie actomyosin structures (phase 1). Interestingly, cell concave edges did not retract simultaneously. After actin bundles contracted, a diffuse actin meshwork became apparent that had condensed actin asters (Figure 6C). Such asters often condensed to form bigger asters. They appeared to be produced by local contractions and ruptures within the diffuse actin meshwork when actin polymerization was inhibited. Interestingly, some breaking events were also recorded in bow-tie actin structures and did not show the healing process. This indicated that actin assembly was also required for the maintenance of a more diffuse actin meshwork that could be the basis for the healing process.

Interestingly, stabilizing actin filaments with Jasplakinolide, drug known to decrease depolymerization rates, led to similar collapse of bridges (data not shown). This effect indicated the necessity for actin depolymerization in stability of bridges and can be explained similarly to LA effect by the depletion of g-actin pools that occurred when actin filaments were no longer disassembling (Cramer, 1999).

MII isoforms localized differentially in bridges with MIIB in the body of bridges and MIIA at the concave edges

To determine whether different myosin isoforms might have different functions in different regions of bridges, we studied the distribution of GFP-labelled MIIA and MIIB in cellular bridges and confirmed the distributions by immunostaining. Both isoforms were concentrated in bridges (Figure 7B), but the distributions were different. MIIB was mainly localized along actin bundles parallel to FN stripes in middle region of the bridges (region 2), whereas MIIA was recruited preferentially to the concave edges (region 1). Furthermore, MIIA showed an enhanced localization in newly formed bridges in which the concave regions 1 were not separated enough to establish the 'bow-tie'-shaped cytoskeleton. Thus, MIIA was the main isoform in the region of high force production, whereas MIIB distributed with actin bundles, maintaining the connection between both ends of bridges.

To determine whether MIIA was a major player in the formation and maintenance of bridges, we transiently depleted MIIA in MEFs with siRNA (Supplementary data and Figure S5) (Cai *et al*, 2006). Control cells were two-fold more likely to form bridges after 30 min compared with the MIIA-depleted ones (Figure 7C). When MIIA-depleted cells spread on patterned substrates (Supplementary Video 15), they developed smaller bridges and the bridging index plateaued after the first 30 min ($Br_i = 0.34$), whereas control cells spread with a constant bridging index ($Br_i = 0.58$, for FN lines of 4.15 μm, gaps of 18.8 μm) (Figure 7C). An interesting observation was that extensions on FN stripes in both control and MIIA knockdown cells were very similar (extension speed: 3.8 μm/min). However, MIIA-depleted cells were not able to expand bridges with the cellular extensions on FN stripes as in control cells (Figure 2B). Such results indicated that extension relied on an MIIA-mediated contraction of the actomyosin meshwork in the concave edge regions, pulling bridges forwards along the FN stripes.

Discussion

In this study, we analysed mechanisms of formation and maintenance of cellular bridges above non-adhesive gaps. Earlier studies *in vivo* (Nishida *et al*, 1988), in 3D environments (Rovensky *et al*, 1999; Thibault and Buschmann, 2006) and on patterned substrates of mixed adhesivity showed that cells can develop bridges whose existence relies on a rich actin meshwork (Lehnert *et al*, 2004; Zimerman *et al*, 2004) with an intact contractility (Chen *et al*, 2003; Thery *et al*, 2006a; Bischofs *et al*, 2008). In our study, we complete this picture by connecting the actin structure of bridges with the dynamics of myosin, the formation of FAs and the production of forces on the substrate. Correlations between these elements have been recognized to be critical in the context of cell motility, but have not been clearly shown with the spatial resolution in these studies.

A major function of fibroblasts in tissues is to secrete or organize collagen and FN fibres by exerting tension on them (Stopak and Harris, 1982). Such force generation by cells in the remodelling of tissues is extremely important in normal (Friedl and Wolf, 2009) as in cancerous tissues (Provenzano *et al*, 2008). Indeed, the remodelling of ECM microenvironment seems now to be a physical signalling event for directional cell migration in tissues. ECM filaments appear to be under constant tension in tissues to create the proper tissue turgor. Such forces would tear the cells apart without counterbalancing forces. We show here that bridges provide such forces continuously through an actomyosin treadmilling process. The highest forces are exerted on the matrix contacts at the ends of the concave edges and concave edges are commonly observed between adhesions even on continuous surfaces. FA grow from contacts in a force-dependent manner, as shown earlier (Balaban *et al*, 2001; Riveline *et al*, 2001; Chen *et al*, 2003). The fact that MIIA localizes to the curved regions where the highest forces are generated is consistent with earlier findings that MIIA localizes at the cell periphery and is responsible for the majority of forces exerted by cells on the matrix (Cai *et al*, 2006). Further, depletion of MIIA results in a reduced ability to bridge non-adhesive gaps. This is consistent with the function of MIIA in the generation of a cohesive actomyosin network for cytoplasmic coherence in MEFs (Cai *et al*, 2010). The fact that a ROCK-dependent pathway of activation of MII is involved in bridge formation is consistent with a recent study showing that, in tumour cells, MRLC associated with MIIA is preferentially activated by ROCK phosphorylation (Sandquist *et al*, 2006). Finally, it seems that force produces a treadmilling flow of actin from the border of the FN stripes towards the non-adhesive area, in the direction of force, with a rate (0.24–0.30 μm/min) similar to observations in dorsal stress fibres on homogeneous FN-coated surfaces (Hotulainen and Lappalainen, 2006). Our results show the direct regulation of assembly by force of a major form of actin at FA where forces are applied as was recently inferred (Endlich *et al*, 2007). Contraction is

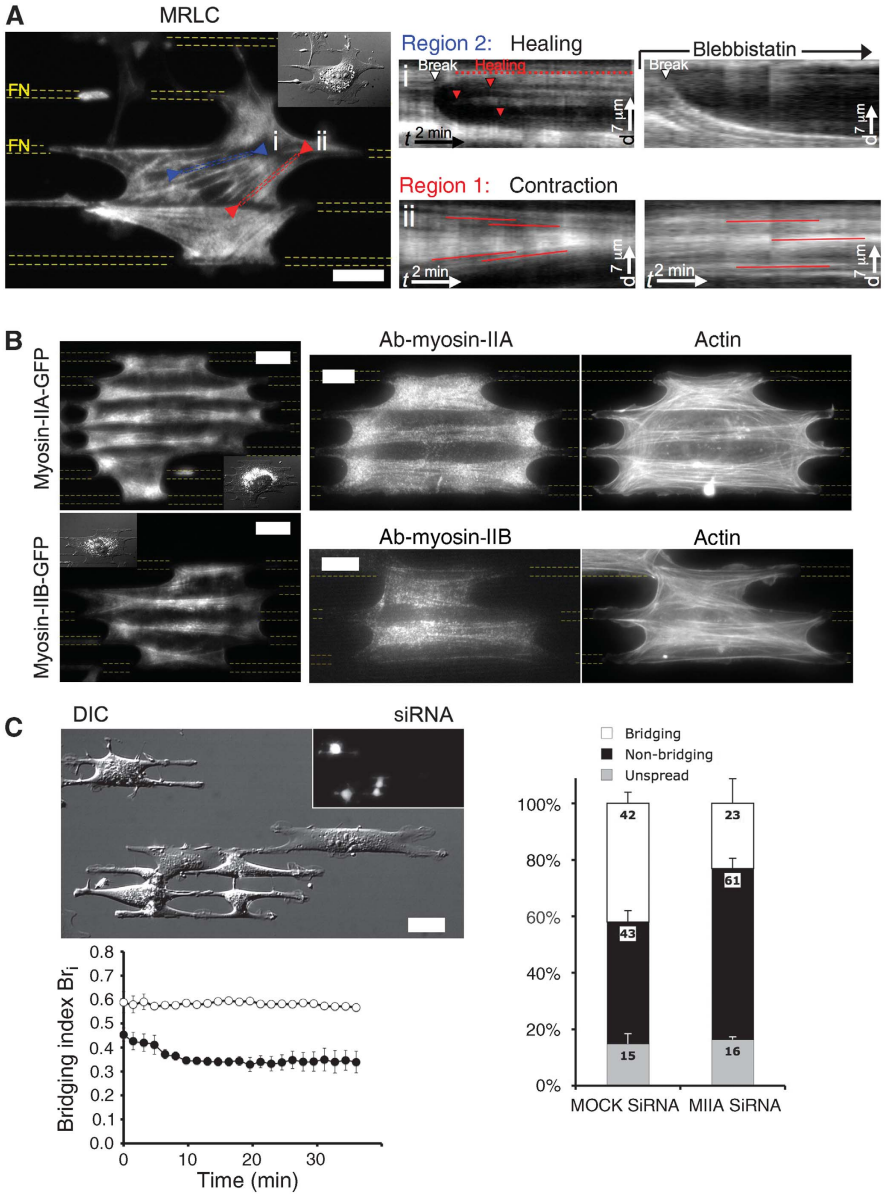

Figure 7 MII isoforms localized differentially in bridges with MIIB in the body of bridges and MIIA at the concave edges. (**A**) GFP-MRLC (TIRF): MII inhibition arrested healing of broken fibres in region 2 and stopped the inwards contractile treadmill of MRLC speckles in region 1. (i) kymograph of MRLC speckles along a breaking actin fibre (blue line i) before and during BBI treatment and (ii) kymograph of MRLC speckles along actin fibre (red line ii) before and during BBI treatment. (**B**) Top panel: MIIA localized at the vicinity of concave edges (region 1) as seen in GFP-MIIA transfected MEFs by TIRF (left) or in MEFs immunostained against MIIA by EPI (right). Bottom panel: MIIB localized in the body of bridges (region 2) as seen in GFP-MIIB transfected MEFs by TIRF (left) or in MEFs immunostained against MIIB by EPI (right). (**C**) Differential interference contrast micrograph of control MEFs and MIIA knockdown MEFs (detected by GFP expression as seen in EPI image in inset) 25 min after plating. Plot of the mean bridging index Br_i versus time during spreading for control MEFs (open circles) and MIIA-depleted cells (closed circles) in differential interference contrast micrograph. Histogram representing the percentage of cells after 30 min on FN stripes, which are displaying bridges (white), spread without bridges (black), and unspread (light grey) for respectively, MEFs treated with Mock siRNA and MIIA siRNA. Scale bars: (**A**, **B**) 15 μm and (**C**) 30 μm.

produced in region 1 where actin filaments assembling at FA are initially all the same polarity. However, rapid filament exchange in a force-independent manner is also observed in our FRAP experiments that could produce filaments of graded polarity (Cramer *et al*, 1997) that would support continuous contraction. Otherwise filaments of opposite polarity could only be bridged by myosin at the crossover region in the middle of the bridge, where anti-parallel filaments interact from the two sides of the bridge. Furthermore, a mechanism in which retrograde flow and MII activity within the leading cell edge delivers F-actin to the lamella to seed the formation of graded polarity actomyosin filament bundles has been described in migrating fibroblasts (Anderson *et al*, 2008). Such a mechanism could occur at the edges of bridges where MII aggregates form with newly assembled actin filaments.

Force could be transduced either indirectly through intermediate signalling molecules that are force dependent such as p130Cas (Sawada *et al*, 2006) or directly through actin polymerization by formins as they are proposed to be 'leaky'

capping proteins. In contrast to the standard capping proteins, formins would allow for actin polymerization in the barbed direction in a force-dependent manner (Kozlov and Bershadsky, 2004). Moreover, mDia1 was shown to be crucial for the actin assembly at FA in stress fibres (Hotulainen and Lappalainen, 2006). Our study indicates that there are direct links between actin assembly, MII contraction, FA formation and force generation on the substrate. The separation of the adhesions from the body of the actomyosin bridges has separated the elements of the system and allowed us to understand how their interplay ensures their self-renewal.

In an adherent state, cells can remodel their cytoskeleton to develop characteristic arc-shape structures that support the cell body between discrete FA. These structures are stable over long periods of time and sustain tension with a dynamic network. How can this stability be maintained in spite of the rapid turnover of all the constituents of the cytoskeleton? The advantage of such turnover is to enable the cell to change its shape (plasticity) depending on the external environment. How the rapid dynamics of the cytoskeleton is linked to the long time stability of the cytoskeleton is much less intuitive. Our observations (Figure 8) suggest that there are additional anti-parallel actin filaments that support the contractile network and the second network of actin seen after latrunculin addition may contribute to this. However, more experiments are needed to determine the basis of this less obvious network. We can say that homeostasis needs constant replenishment of the cytoskeleton through actin polymerization and myosin contraction.

Initially, matrix-dependent cell spreading can extend over non-adhesive or soft surfaces, even with cells lacking talin (Giannone *et al*, 2004; Zhang *et al*, 2008). When contraction starts, cells exert contractile force on matrix where FA sites will grow and create inwards curved edges over non-adhesive regions, based on the matrix geometry *per se*. Many earlier studies have noted the loss of force on the inhibition of MII, but did not find a similar collapse of cytoplasm because the surfaces were generally more adhesive. Continuous adhesive regions will support extension of cell processes by an MII-independent process.

Our experimental device presents clear advantages for the study of the relation between cytoskeleton plasticity and stability. In other patterned substrates with small islands or dots, wide bridging structures are also generated, but they are of limited length (Chen *et al*, 1997, 2003; Lehnert *et al*, 2004; Bischofs *et al*, 2008). The linear geometry provides a mixed adhesivity under the whole cell area, without limiting the area on which they can develop contacts with the substrate. Hence, with large bridges, we have been able to clearly identify two types of regions within spread cells in which actomyosin structures are organized differently and seem to perform different functions. The reproducibility of this pattern allows the clear identification of a control phenotype. Altering actin polymerization or myosin contractility causes

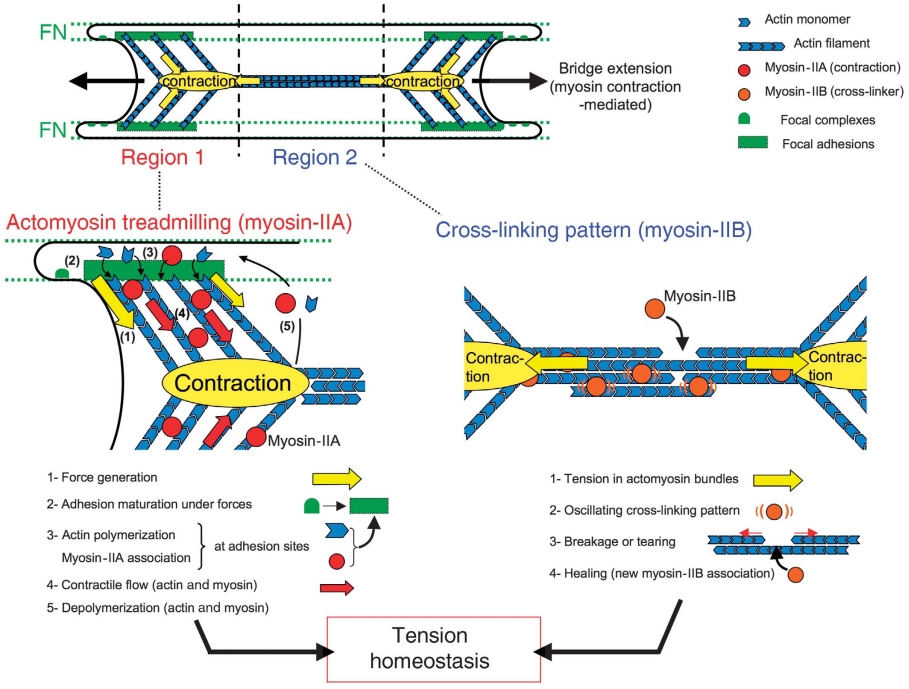

Figure 8 Working model of the maintenance and translocation of cellular bridges controlled by actomyosin contraction. Bridges between the FN stripes have a 'bow-tie'-shaped actin cytoskeleton. Such organization is maintained in regions 1 by MIIA-based continuous actomyosin treadmilling pattern located at the concave edges (contraction nodes are represented with yellow ovals) and in region 2 by a 'cross-linking' pattern in the body of bridges. Extensions on FN stripes provide new FA sites, which serve as anchors for bridges' actomyosin meshwork to translocate using contraction-generated forces. The sequence of events in regions 1 are (1) generation of forces (yellow arrows) on FN stripes, which induce (2) maturation of adhesions on edges of FN stripes (green rectangle), (3) forces localize at FAs sites, the turnover of actin (blue chevron) and subsequent MII (red circles) association, which maintain the (4) contractile treadmilling flow (red arrow) of actin and MII from FN stripes towards non-adhesive area. In the region 2, actomyosin bundles are pulled on both sides by contractions in regions 1 (yellow arrows). This induces (1) tension in actomyosin bundles observed through (2) oscillating 'cross-linking' pattern of MII (orange circles) and α-actinin. When tension is too high, cross-links ruptured and bundles are tearing until (3) MII-based healing process during which new MIIB cross-linkers associate and restore the mechanical continuity. Such process confers tensional homeostasis to the dynamic meshwork.

bridge collapse. This collapse in both cases is a consequence of membrane tension reminiscent of soap film behaviour and not of some other motor than MII. Indeed, during LA treatment, the actin bundles detach, and are quickly condensed by MII, whereas the edge is supported by a second actomyosin network. Then, after further actomyosin contraction of the remaining network, concave edges are no longer supported and retract. During BBI treatment, loss of forces also induces loss of actomyosin bundles and perhaps the second actomyosin network that causes concave edges to retract without the transient extension observed with LA. Assuming a membrane tension of cell plasma membrane of 0.1 mN/m (Sheetz, 2001), and a distance of the gap between the FN stripes ($\sim$10 μm), tension along the unsupported concave edge would be $\sim$1 nN that is slightly below the force level of a native FA. As bridges are actively translocating the cell body by contraction and simultaneously maintaining the cell coherence (Cai and Sheetz, 2009), they can be essential structures for migration in 3D environments. Indeed, the choice of linear geometry for adhesive regions approximates the linear organization of ECM fibres (FN, collagen), which present linear sites of potential integrin-mediated adhesion. Such fibres (diameter range: 500–1000 nm spaced by 5–10 μm) can be found *in vivo* in stromal tissues, as observed in the cornea (Nishida *et al*, 1988).

Model of tensional homeostasis through actomyosin treadmilling and cross-linking

From our studies as well as others that have shown force-dependent actin assembly and dynamics, a model emerges to explain how cells can sustain tension on FA sites with a dynamic actomyosin network. There is assembly of both myosin and actin filaments at or near FA sites and disassembly at the middle of the non-adhesive regions that constitutes a treadmilling process to renew the network and sustain tension over long periods, while allowing adjustments. MII-catalysed assembly of the connecting bridges is remarkable in that MII contraction is needed for the continued assembly and inwards movement of both actin and myosin filaments. Movement of assembled myosin filaments away from actin assembly regions could explain the relative depletion of MII from FA sites that has been observed on homogeneous adhesive substrates (Giannone *et al*, 2007). This interplay between continuous contraction and force-stimulated actin assembly enables movement of tense actomyosin structures without loss of tension or the disruption of cytoplasm by matrix forces.

Owing to the large distance between adhesions, repair of the network is critical. To provide mechanical coherence by an MII-based actin cross-linking activity, there must also be a healing mechanism or breaks such as those caused by LA would cause frequent large retractions. When breaks occur, there is an initial recoil and then new filaments form and restore the mechanical continuity. This healing feature of the networks is particularly striking in contrast with the super-precipitation of actomyosin networks *in vitro* (Janson and Taylor, 1993).

In this model, we suggest that MII contraction acts at two levels to maintain the cellular bridges: (1) by catalysing actin assembly at FA contacts and (2) by stabilizing the filament network by cross-linking. In summary, MIIA-based contraction is necessary to set in motion the sequence of events that establishes bridges (Figure 8). As similar movements and similar morphologies are observed in different cell types, we suggest that these are general cell responses to discontinuous adhesions. This study provides quantitative measures of the dynamic properties of the cytoskeleton that provide the basis for stable force generation and plasticity over time.

Materials and methods

Cell culture, plasmids and transfection

Immortalized MEFs (Giannone *et al*, 2004, 2007) and mouse fibroblasts NIH 3T3 (ATCC) were maintained in DMEM medium (Gibco) supplemented with 10% FBS (Gibco), 1% L-glutamine and 100 IU/mg penicillin-streptomycin (Invitrogen) at 37°C and 5% CO_2.

Plasmids included EGFP-MRLC and monomeric red fluorescent protein (mRFP)-MRLC (Tamada *et al*, 2007), as well as mRFP-β-actin and human EGFP-β-actin (Boyer *et al*, 2006), EGFP-α-actinin (provided by CA Otey), GFP-integrin β3 (Plancon *et al*, 2001), GFP-labelled MIIA and MIIB (Wei and Adelstein, 2000), pmaxGFP (Lonza) and mCherry (Clontech). The plasmids used to express hairpin short-interfering RNA (MIIA siRNA) targeting mouse non-muscle MIIA as well as a control plasmid (Mock siRNA) encoding a hairpin siRNA whose sequence is not found in the mouse databases (provided by Ambion) were described elsewhere (Cai *et al*, 2006).

Transient transfection of plasmids was performed through electroporation using a Nucleofector (Lonza) 1 to 2 days before an experiment according to the manufacturer's protocol (MEF-1 solution and program T-20), except for the case of siRNA plasmids in which cells were used 2 to 4 days after electroporation to ensure 85% reduction of protein levels (Cai *et al*, 2006).

Antibodies and materials

Polyclonal rabbit antibody against the heavy chain of MIIA was obtained as a gift from Dr Robert Adelstein (National Institutes of Health, Bethesda). mAb against non-muscle MIIB (clone CMII 23) was from Developmental Studies, Hybridoma Bank (University of Iowa, Iowa City). mAb anti-paxillin was purchased from BD Transduction Laboratories (San Jose). All fluorophore-conjugated secondary antibodies were from Molecular Probes. (±)-BBI, Y-27632, ML-7 and LA were purchased from Calbiochem. Full-length human FN was purchased from Roche. 1-Octadecanethiol, Pluronic F-127 and anhydrous ethanol were purchased from Sigma. PEG-terminated thiols were purchased from ProChimia (Poland).

Live-cell imaging

MEFs were plated 24 h before an experiment at 80 000 cells per 1.5 cm tissue culture dish, harvested and added to substrates at 100 000 cells/ml in Ringer 1 solution (150 mM NaCl, 5 mM KCl, 1 mM $CaCl_2$, 1 mM $MgCl_2$, 20 mM Hepes and 2 g/l glucose, pH 7.4). Cells were imaged at 37°C with an Olympus IX81 TIRF microscope (Olympus) coupled to a Coherent Innova 70C-Spectrum multi-wavelength laser (Coherent). Time-lapse micrographs were recorded with a 20× air objective (UplanApo 0.7NA) or a 60× oil immersion objective (PlanApo TIRFM 1.45 NA) through a cooled CCD camera CoolSNAP HQ (Roper Scientific Inc.) using Simple PCI software (Compix Inc.). The same setup was used for TIRF microscopy as well as in EPI experiments with either the laser or direct Hg lamp excitation. In the case of acute drug treatments, cells were allowed to spread for 45–60 min before perfusion of 50 μM BBI, 25 μM Rho-kinase inhibitor Y-27632, 10 μM ML-7 (MLCK-specific inhibitor) or 200 nM LA, and images were typically acquired every 2–10 s for up to 3 h. Image analysis was performed using the open-source image-analysis program NIH ImageJ (developed by W Rasband, National Institute of Health, Bethesda, MD, USA). The plugin SpotTracker (Sage *et al*, 2005) was used for its optimal filter to enhance a Gaussian-like fluorescent spot, whereas attenuating the background noise (spot diameter parameter: 1.25pixel).

Immunofluorescence

Cells were incubated at 37°C on patterned substrates at a density of 40 000 cells/ml for 90 min in the different conditions (control, BBI treated, Y-27632 treated, ML-7 treated or LA treated), and then fixed with 3.7% (vol/vol) formaldehyde in PBS, and permeabilized with

0.1% Triton X-100 in PBS for 4 min. Cells were incubated for 20 min with AlexaFluor 568 phalloidin (Molecular Probes) to visualize F-actin. Samples were mounted in PBS to allow imaging by both EPI and TIRF microscopy.

Statistical analysis

Statistical differences between different conditions were assessed with a two-tailed Student's *t*-test and the level of significance was taken to be $P<0.01$. All errors are given as ± standard error (s.e.m.).

Supplementary data

Supplementary data are available at *The EMBO Journal* Online (http://www.embojournal.org).

Acknowledgements

We thank M Tamada for MRLC-EGFP, MRLC-mRFP and, mRFP-β-actin, and L Boyer, C Otey and E Marcantonio for providing us with EGFP-β-actin, α-actinin-GFP, GFP-paxillin constructs, respectively, and M Smith and V Vogel for providing us with fluorescently-labelled fibronectin. G Giannone provided helpful discussions, and S Moore, B Dubin-Thaler and T Perez for critical review of the paper. This work was supported by grants from the National Institutes of Health through the NIH Roadmap for Medical Research (PN2 EY016586) to MPS.

Conflict of interest

The authors declare that they have no conflict of interest.

References

Anderson TW, Vaughan AN, Cramer LP (2008) Retrograde flow and myosin II activity within the leading cell edge deliver F-actin to the lamella to seed the formation of graded polarity actomyosin II filament bundles in migrating fibroblasts. *Mol Biol Cell* **19:** 5006–5018

Balaban NQ, Schwarz US, Riveline D, Goichberg P, Tzur G, Sabanay I, Mahalu D, Safran S, Bershadsky A, Addadi L, Geiger B (2001) Force and focal adhesion assembly: a close relationship studied using elastic micropatterned substrates. *Nat Cell Biol* **3:** 466–472

Bischofs IB, Klein F, Lehnert D, Bastmeyer M, Schwarz US (2008) Filamentous network mechanics and active contractility determine cell and tissue shape. *Biophys J* **95:** 3488–3496

Boyer L, Doye A, Rolando M, Flatau G, Munro P, Gounon P, Clement R, Pulcini C, Popoff MR, Mettouchi A, Landraud L, Dussurget O, Lemichez E (2006) Induction of transient macroapertures in endothelial cells through RhoA inhibition by Staphylococcus aureus factors. *J Cell Biol* **173:** 809–819

Cai Y, Biais N, Giannone G, Tanase M, Jiang G, Hofman JM, Wiggins CH, Silberzan P, Buguin A, Ladoux B, Sheetz MP (2006) Nonmuscle myosin IIA-dependent force inhibits cell spreading and drives F-actin flow. *Biophys J* **91:** 3907–3920

Cai Y, Rossier O, Gauthier N, Biais N, Fardin M-A, Zhang X, Miller LW, Ladoux B, Cornish VW, Sheetz MP (2010) Cytoskeletal coherence requires myosin IIA contractility. *J Cell Sci* **123:** 413–423

Cai Y, Sheetz MP (2009) Force propagation across cells: mechanical coherence of dynamic cytoskeletons. *Curr Opin Cell Biol* **21:** 47–50

Chen CS, Alonso JL, Ostuni E, Whitesides GM, Ingber DE (2003) Cell shape provides global control of focal adhesion assembly. *Biochem Biophys Res Commun* **307:** 355–361

Chen CS, Mrksich M, Huang S, Whitesides GM, Ingber DE (1997) Geometric control of cell life and death. *Science* **276:** 1425–1428

Conti MA, Adelstein RS (2008) Nonmuscle myosin II moves in new directions. *J Cell Sci* **121:** 11–18

Cramer LP (1999) Role of actin-filament disassembly in lamellipodium protrusion in motile cells revealed using the drug jasplakinolide. *Curr Biol* **9:** 1095–1105

Cramer LP, Siebert M, Mitchison TJ (1997) Identification of novel graded polarity actin filament bundles in locomoting heart fibroblasts: implications for the generation of motile force. *J Cell Biol* **136:** 1287–1305

Desaki J, Shimizu M (2000) A re-examination of the cellular reticulum of fibroblast-like cells in the rat small intestine by scanning electron microscopy. *J Electron Microsc (Tokyo)* **49:** 203–208

Doyle AD, Wang FW, Matsumoto K, Yamada KM (2009) One-dimensional topography underlies three-dimensional fibrillar cell migration. *J Cell Biol* **184:** 481–490

Endlich N, Otey CA, Kriz W, Endlich K (2007) Movement of stress fibers away from focal adhesions identifies focal adhesions as sites of stress fiber assembly in stationary cells. *Cell Motil Cytoskeleton* **64:** 966–976

Friedl P, Brocker EB (2000) The biology of cell locomotion within three-dimensional extracellular matrix. *Cell Mol Life Sci* **57:** 41–64

Friedl P, Wolf K (2009) Plasticity of cell migration: a multiscale tuning model. *J Cell Biol* **188:** 11–19

Galbraith CG, Sheetz MP (1997) A micromachined device provides a new bend on fibroblast traction forces. *Proc Natl Acad Sci USA* **94:** 9114–9118

Galbraith CG, Yamada KM, Sheetz MP (2002) The relationship between force and focal complex development. *J Cell Biol* **159:** 695–705

Giannone G, Dubin-Thaler BJ, Dobereiner HG, Kieffer N, Bresnick AR, Sheetz MP (2004) Periodic lamellipodial contractions correlate with rearward actin waves. *Cell* **116:** 431–443

Giannone G, Dubin-Thaler BJ, Rossier O, Cai Y, Chaga O, Jiang G, Beaver W, Dobereiner HG, Freund Y, Borisy G, Sheetz MP (2007) Lamellipodial actin mechanically links myosin activity with adhesion-site formation. *Cell* **128:** 561–575

Goffin JM, Pittet P, Csucs G, Lussi JW, Meister JJ, Hinz B (2006) Focal adhesion size controls tension-dependent recruitment of alpha-smooth muscle actin to stress fibers. *J Cell Biol* **172:** 259–268

Hotulainen P, Lappalainen P (2006) Stress fibers are generated by two distinct actin assembly mechanisms in motile cells. *J Cell Biol* **173:** 383–394

Janson LW, Taylor DL (1993) *In vitro* models of tail contraction and cytoplasmic streaming in amoeboid cells. *J Cell Biol* **123:** 345–356

Jester JV, Barry PA, Lind GJ, Petroll WM, Garana R, Cavanagh HD (1994) Corneal keratocytes: *in situ* and *in vitro* organization of cytoskeletal contractile proteins. *Invest Ophthalmol Vis Sci* **35:** 730–743

Jester JV, Petroll WM, Cavanagh HD (1999) Corneal stromal wound healing in refractive surgery: the role of myofibroblasts. *Prog Retin Eye Res* **18:** 311–356

Kozlov MM, Bershadsky AD (2004) Processive capping by formin suggests a force-driven mechanism of actin polymerization. *J Cell Biol* **167:** 1011–1017

Kumar S, Maxwell IZ, Heisterkamp A, Polte TR, Lele TP, Salanga M, Mazur E, Ingber DE (2006) Viscoelastic retraction of single living stress fibers and its impact on cell shape, cytoskeletal organization, and extracellular matrix mechanics. *Biophys J* **90:** 3762–3773

Lehnert D, Wehrle-Haller B, David C, Weiland U, Ballestrem C, Imhof BA, Bastmeyer M (2004) Cell behaviour on micropatterned substrata: limits of extracellular matrix geometry for spreading and adhesion. *J Cell Sci* **117:** 41–52

Medeiros NA, Burnette DT, Forscher P (2006) Myosin II functions in actin-bundle turnover in neuronal growth cones. *Nat Cell Biol* **8:** 216–226

Meshel AS, Wei Q, Adelstein RS, Sheetz MP (2005) Basic mechanism of three-dimensional collagen fibre transport by fibroblasts. *Nat Cell Biol* **7:** 157–164

Mitchison TJ (1992) Actin based motility on retraction fibers in mitotic PtK2 cells. *Cell Motil Cytoskeleton* **22:** 135–151

Nishida T, Yasumoto K, Otori T, Desaki J (1988) The network structure of corneal fibroblasts in the rat as revealed by scanning electron microscopy. *Invest Ophthalmol Vis Sci* **29:** 1887–1890

Plancon S, Morel-Kopp MC, Schaffner-Reckinger E, Chen P, Kieffer N (2001) Green fluorescent protein (GFP) tagged to the cytoplasmic tail of alphaIIb or beta3 allows the expression of a

fully functional integrin alphaIIb(beta3): effect of beta3GFP on alphaIIb(beta3) ligand binding. *Biochem J* **357:** 529–536

Ponti A, Machacek M, Gupton SL, Waterman-Storer CM, Danuser G (2004) Two distinct actin networks drive the protrusion of migrating cells. *Science* **305:** 1782–1786

Provenzano PP, Inman DR, Eliceiri KW, Trier SM, Keely PJ (2008) Contact guidance mediated three-dimensional cell migration is regulated by Rho/ROCK-dependent matrix reorganization. *Biophys J* **95:** 5374–5384

Rajfur Z, Roy P, Otey C, Romer L, Jacobson K (2002) Dissecting the link between stress fibres and focal adhesions by CALI with EGFP fusion proteins. *Nat Cell Biol* **4:** 286–293

Riveline D, Zamir E, Balaban NQ, Schwarz US, Ishizaki T, Narumiya S, Kam Z, Geiger B, Bershadsky AD (2001) Focal contacts as mechanosensors: externally applied local mechanical force induces growth of focal contacts by an mDia1-dependent and ROCK-independent mechanism. *J Cell Biol* **153:** 1175–1186

Rovensky YA, Domnina LV, Ivanova OY, Vasiliev JM (1999) Locomotory behaviour of epitheliocytes and fibroblasts on metallic grids. *J Cell Sci* **112**(Pt 8)**:** 1273–1282

Sage D, Neumann FR, Hediger F, Gasser SM, Unser M (2005) Automatic tracking of individual fluorescence particles: application to the study of chromosome dynamics. *IEEE Trans Image Process* **14:** 1372–1383

Sandquist JC, Swenson KI, Demali KA, Burridge K, Means AR (2006) Rho kinase differentially regulates phosphorylation of nonmuscle myosin II isoforms A and B during cell rounding and migration. *J Biol Chem* **281:** 35873–35883

Sawada Y, Tamada M, Dubin-Thaler BJ, Cherniavskaya O, Sakai R, Tanaka S, Sheetz MP (2006) Force sensing by mechanical extension of the Src family kinase substrate p130Cas. *Cell* **127:** 1015–1026

Schnell E, Klinkhammer K, Balzer S, Brook G, Klee D, Dalton P, Mey J (2007) Guidance of glial cell migration and axonal growth on electrospun nanofibers of poly-[epsilon]-caprolactone and a collagen/poly-[epsilon]-caprolactone blend. *Biomaterials* **28:** 3012–3025

Sheetz MP (2001) Cell control by membrane-cytoskeleton adhesion. *Nat Rev Mol Cell Biol* **2:** 392–396

Sims JR, Karp S, Ingber DE (1992) Altering the cellular mechanical force balance results in integrated changes in cell, cytoskeletal and nuclear shape. *J Cell Sci* **103**(Pt 4)**:** 1215–1222

Stoitzner P, Pfaller K, Stossel H, Romani N (2002) A close-up view of migrating langerhans cells in the skin. *J Invest Dermatol* **118:** 117–125

Stopak D, Harris AK (1982) Connective tissue morphogenesis by fibroblast traction : I. Tissue culture observations. *Dev Biol* **90:** 383–398

Straight AF, Cheung A, Limouze J, Chen I, Westwood NJ, Sellers JR, Mitchison TJ (2003) Dissecting temporal and spatial control of cytokinesis with a myosin II Inhibitor. *Science* **299:** 1743–1747

Tamada M, Perez TD, Nelson WJ, Sheetz MP (2007) Two distinct modes of myosin assembly and dynamics during epithelial wound closure. *J Cell Biol* **176:** 27–33

Tan JL, Tien J, Pirone DM, Gray DS, Bhadriraju K, Chen CS (2003) Cells lying on a bed of microneedles: an approach to isolate mechanical force. *Proc Natl Acad Sci USA* **100:** 1484–1489

Thery M, Pepin A, Dressaire E, Chen Y, Bornens M (2006a) Cell distribution of stress fibres in response to the geometry of the adhesive environment. *Cell Motil Cytoskeleton* **63:** 341–355

Thery M, Racine V, Piel M, Pepin A, Dimitrov A, Chen Y, Sibarita JB, Bornens M (2006b) Anisotropy of cell adhesive microenvironment governs cell internal organization and orientation of polarity. *Proc Natl Acad Sci USA* **103:** 19771–19776

Thibault MM, Buschmann MD (2006) Migration of bone marrow stromal cells in 3D: 4 color methodology reveals spatially and temporally coordinated events. *Cell Motil Cytoskeleton* **63:** 725–740

Toyoda H, Ina K, Kitamura H, Tsuda T, Shimada T (1997) Organization of the lamina propria mucosae of rat intestinal mucosa, with special reference to the subepithelial connective tissue. *Acta Anat* **158:** 172–184

Wang N, Ingber DE (1994) Control of cytoskeletal mechanics by extracellular matrix, cell shape, and mechanical tension. *Biophys J* **66:** 2181–2189

Watanabe N, Mitchison TJ (2002) Single-molecule speckle analysis of actin filament turnover in lamellipodia. *Science* **295:** 1083–1086

Wei Q, Adelstein RS (2000) Conditional expression of a truncated fragment of nonmuscle myosin II-A alters cell shape but not cytokinesis in HeLa cells. *Mol Biol Cell* **11:** 3617–3627

Yumura S, Mori H, Fukui Y (1984) Localization of actin and myosin for the study of ameboid movement in Dictyostelium using improved immunofluorescence. *J Cell Biol* **99:** 894–899

Zand MS, Albrecht-Buehler G (1989) What structures, besides adhesions, prevent spread cells from rounding up? *Cell Motil Cytoskeleton* **13:** 195–211

Zhang X, Jiang G, Cai Y, Monkley SJ, Critchley DR, Sheetz MP (2008) Talin depletion reveals independence of initial cell spreading from integrin activation and traction. *Nat Cell Biol* **10:** 1062–1068

Zimerman B, Arnold M, Ulmer J, Blummel J, Besser A, Spatz JP, Geiger B (2004) Formation of focal adhesion-stress fibre complexes coordinated by adhesive and non-adhesive surface domains. *IEE Proc Nanobiotechnol* **151:** 62–66

